Journal of Electrical Engineering, Vol. 74, No. 4, 2023, pp. 293-301

sciendo

PAPER

A miniaturized quintuple-band frequency selective surface based on enclosed cross slots

Pratyancha Prasad and Akhilesh Kumar

This article presents a low-profile quintuple-band frequency selective surface (FSS) that is designed as a sub-reflector for applications including satellite systems (C band), EPR (electron paramagnetic resonance) spectrometers, motion and traffic light crossing detectors (X band), Direct Broadcast Satellite and broadcasting satellite service (Ku band), and shortrange applications (K band). The dimensions of the miniaturized unit cell $0.08\lambda_0 \times 0.08\lambda_0 \times 0.012\lambda_0$, where, λ_0 is the free-space wavelength corresponding to the lower cut-off frequency. There are five stop bands, and frequencies at which they resonate are 6.3, 7.06, 9.30, 11.2, 14.0, and 18.64 GHz. The fractional bandwidths (FBW) of these bands are 62.6, 7.5, 9.2, 11, and 11.69%, respectively. Additionally, as a result of the structure's four-fold symmetry, it exhibits a good polarization-insensitive response as well as a stable response in both the TE and TM modes. Full-wave simulation is performed on the structure, after which an equivalent circuit model is constructed.

Keywords: frequency selective surface (FSS), quintuple band, multiband operations, miniaturization

1. Introduction

Frequency selective surfaces, also known as FSS, are periodic arrays, typically in two dimensions, that are made up of geometric elements such as patches or slots, and they are typically printed on a dielectric substrate. FSSs may display band stop characteristics, band pass characteristics, or a combination of both of these types of characteristics. FSS are frequently used in a variety of applications, including antennas interfaces, filters, polarizers, randoms, and absorbers, to name a few [1,2]. With the rapid development of today's communication systems, multiband communications have become increasingly important because they provide the necessary flexibility to run multiple frequencies and multiple standards of application simultaneously. Recent research in multiband FSS has been motivated by the coexistence of various wireless communication systems that operate at various nearby operating bands as well as systems that use more than one band in concurrent mode. These systems include both single-band systems and systems that use more than one band simultaneously. Because of the need to make efficient use of the radioelectric spectrum, the frequency band allocations of these wireless communication systems are closely spaced. As a result, the problem of electromagnetic compatibility arises when these multifrequency and multistranded systems operate in contiguous locations, producing elevated levels of electromagnetic interference (EMI). These systems can reap the benefits of multiband FSSs with transmission bands that are closely spaced from one another and provide appropriate band isolation to prevent electromagnetic interference (EMI) between systems or subsystems that operate in frequency bands that are located nearby. Therefore, multi-bandpass FSS can be utilized efficiently to protect locations, systems, or circuits from unwelcome radio frequency (RF) signals while yet facilitating the transmission of messages that are needed. It is essential to note some of the applications of the multi-bandpass FSS, such as preventing EMI between radar and satellite communication antenna [3], electromagnetic architecture of buildings [4, 5], and band isolation in systems working in concurrent mode [6].

Combining multiple resonators in the unit cell has been commonly employed in the past to achieve a multi-band FSS. Due to the close closeness of the intense electromagnetic fields that arise at resonances, this technique suffers from a significant mutual coupling between adjacent resonators. A mutual coupling reduction must be implemented in order to produce the desired near band response. It is possible to provide a tiny spacing between adjacent bands by combining several ring loop designs (metal patches and apertures). Due to their near proximity, a big separation in frequency is caused by an increase in the mutual coupling between their resonances as their distances decrease. This result makes it difficult to achieve a close band design. The geometry of the ring loops must therefore be modified to reduce the mutual coupling significantly.

Multiple strategies like multi-resonant elements, loaded element FSS, cascading layers, fractal structures, perturbed FSS, and loaded element FSS, etc have been used in the closely spaced multiband FSS design to increase the multiband FSS' performance. While initially applied to systems with only two bands [7-9], these methods are now being used in systems with many more bands.

In [10], a highly selective quad-band operation was accomplished by cascading three metallic layers. This was done to produce the desired result. These three layers of metallic material are encased within two substrate layers that are located in between them. Even if cascading is a possibility for achieving multiband operation, the fabrication process for doing so is complicated, and the resulting device is not a miniaturized one.

Now, fractal geometry [11] or convoluted structure [12] can be used to enable multi-band operating in a smaller version. Also, another intriguing strategy for reducing size is to load active elements onto the FSS [13,14] or to insert vias [15] to tune

Department of Electronics and Communication Engineering, National Institute of Technology, Jamshedpur, India
pratyancha.p17@gmail.com

https://doi.org/10.2478/jee-2023-0036, Print (till 2015) ISSN 1335-3632, On-line ISSN 1339-309X

the resonant frequency. Both of these strategies can be found in the references. Nevertheless, the intricacy of the fabrication will rise when using either of these methods.

In situations when these methods are not an option, one of the most common approaches to achieving multi-band functioning with a single-layered design is to make use of parts with several resonant modes. On a single layered FSS, it has been possible to accomplish tri-band [16], quad-band [17-19], and recently, various penta-band designs consisting of bands that are situated in close proximity have been researched. Combining an adjacent loop interconnection method with an arrow-shaped ring in the outermost loop results in five stopbands, as shown in the publication [20]. Next, a penta-band stop FSS is built by employing several distinct variants on a squared ring [21]. A later paper, [22], detailed a two-layer, penta-band stop FSS that made use of five metallic structures. Two metal structures were found on one side of the dielectric, whereas three were found on the other. Recently, a five stopband FSS was developed by integrating different loop geometries in the unit cell, such as circles and squares, as reported in [23]. In [24] presents a penta-bandpass FSS that utilizes slot resonators arranged in concentric rings.

- This paper presents a quintuple band FSS that is two-dimensional, has a metallization layer that is present on both sides, and has resonance frequencies of 6.3 and 7.06, 9.30 and 11.2, 14.0 and 18.64 GHz, respectively. The upper conductive layer of the envisioned four-fold configuration is made up of concentric enclosed cross slots, which are responsible for the five bandstop response.
- On the other hand, the motivation behind putting the lower conductive layer, which is an optimized square ring, is high selectivity between bands.
- A miniaturized unit cell dimension $0.08\lambda_0 \times 0.08\lambda_0 \times 0.012\lambda_0$, where, λ_0 is the free-space wavelength corresponding to the lower cut-off frequency.
- Both polarization independence (TM) and angular stability (TE) are maintained by the model up to an incidence angle of 75^0.

In order to validate the realized structure and equivalent circuit model, a full wave solver high frequency structure simulator (HFSS) is utilized. This allows for the model to be checked for accuracy. The remaining sections of the paper are structured in the following manner. The construction of the unit cell as well as an explanation of its function can be found in Section II. Analyses of various factors followed by the Iterations and Results Discussion in Section III. Experimental confirmation can be found in section IV. Section V, the conclusion, which is the very last part of the whole piece of work.

2. Unit cell design

The proposed unit cell features a design that incorporates a two-sided metallic layer that is printed on a FR-4 substrate. The layer has a thickness of 0.8 mm ($0.012\lambda_0$), a relative permittivity (ϵr) of 4.4, and a loss tangent of 0.02. The overall FSS is organized in such a way that the length (x-axis), width (y-axis), and height (z-axis) of the structure match, respectively, to the x, y, and z axes of the structure. Utilizing HFSS software allows for the purpose of achieving the goal of acquiring the final parameters of the planned FSS.

The front side, the rear side, and the side view of the unit cell are depicted, respectively, in Figure 1(a), 1(b), and 1(c). The primary objective of the proposed FSS is to realize various stop and pass bands across the whole frequency range up to 20 GHz.

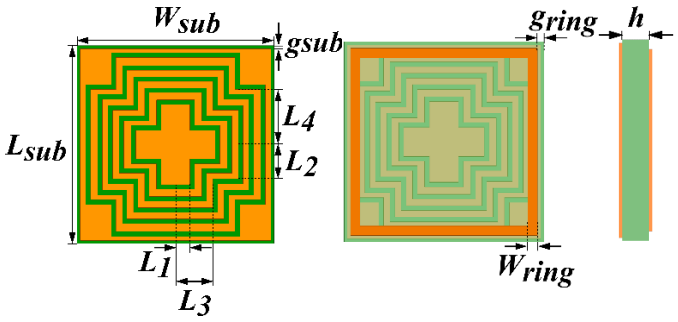

Fig. 1. Unit cell (a) front view, (b) rear view, and (c) side view.

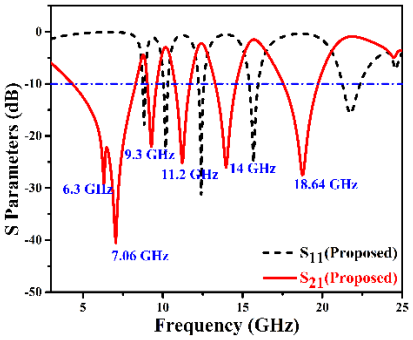

Fig. 2. S parameters of proposed structure.

Figure 2 depicts the transmission (S_{21}) and reflection (S_{11}) characteristics of FSS for TE polarization at the normal angle of incidence for quintuple stop bands (4.34 – 8.30 GHz, 9.04 – 9.62 GHz, 10.76 – 11.70 GHz, 13.20 – 14.60 GHz, and 17.55 – 19.73 GHz) and quintuple pass bands (8.74 – 8.95 GHz, 10.05 – 10.5 GHz, 12.0 – 12.64 GHz, 15.40 – 15.95 GHz and 21.01 – 22.32 GHz. The frequency of the primary resonant mode is influenced by the cross slot that is located furthest from the centre and has the largest perimeter, and vice versa. The optimized parameters are as follow (unit in mm): $W_{sub} = L_{sub} = 6.2$, $g_{sub} = 0.1$, $g_{slot} = 0.15$, $g_{ring} = 0.2$, $W_{slot} = 0.22$ (width of slot), $W_{ring} = 0.3$, $L_1 = 0.45$, $L_2 = 0.82$, $L_3 = 1.17$, $L_4 = 1.52$, $L_5 = 1.87$, and $h = 0.8$.

3. Iterations and results

Figure 3 presents a visual representation of the iterations of the multiband FSS unit cell. It has been found that the resultant resonances and bandwidths of each band in the overall system change as a direct consequence of the mutual coupling that takes place between neighbouring enclosed slots at various phases. This was discovered after it was found that the resultant resonances and bandwidths of each band in the overall system change.

To begin, the first enclosed cross slot that contributes to the first stop band frequency ranges from 4.70 to 7.14 GHz and has the greatest perimeter. Its resonant frequency is measured at 6.31 GHz, and its fractional bandwidth (FBW) for 41.2%. After the second slot has been implemented with the width and spacing optimized, the second stop band will arise at 9.13- 9.70 GHz, and its resonant frequency will be 9.41 GHz. This will occur after the second stop band has been implemented. Additionally, as a result of the mutual relationship with the first band, some subtle changes take place within the band. Now, adding one more band with a resonance frequency of 11.37 GHz requires merging the prior FSS design with the third cross slot from the preceding design. This new band utilizes a frequency spectrum that stretches from 10.95 to 11.82 GHz and has a FBW of 7.6%. By adding two extra slot structures to the arrangement from before, it is possible to construct an additional two stop bands during the fourth and fifth iterations of the process. As a consequence of this, the resonance frequencies come out to be 14.01 GHz and 18.84 GHz. These two new band frequencies have a FBW of 8.5 percent and 9.6%, and they span from 13.40-14.60 GHz and 7.83-19.63 GHz, respectively. In the final iteration, by adding a square ring with optimized width as a lower conductive layer at the back side of the substrate layer, there is a significant improvement in the proposed structure in terms of selectivity and bandwidth across the entire range shown in Table 1. In this iteration, the proposed structure was significantly improved.

This section investigates how changing the dimensions of the responsible parameters that generate resonant affects the frequency response of the proposed penta-bandstop FSS. These responsible parameters include the distance between each of the slots (g_{slot}), the distance between the substrate and the conductive layer (g_{subs}), height of the substate (h) and width of the ring (w_{ring}) as shown in Figure 4.

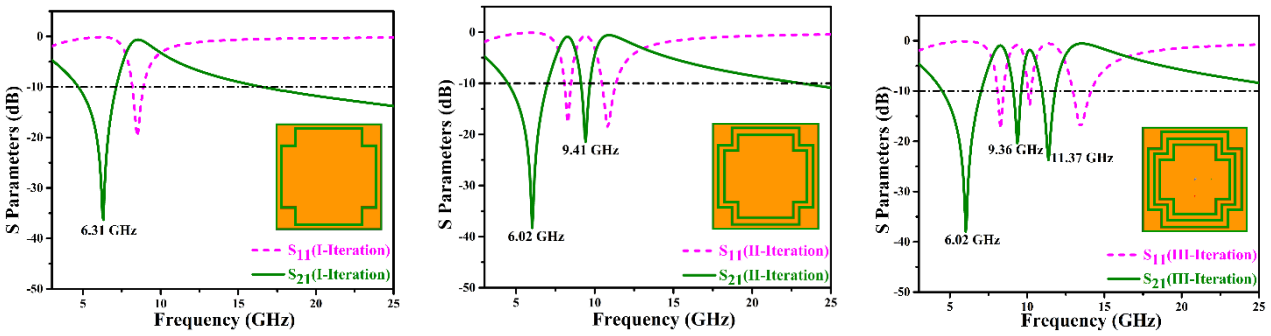

(a) (b) (c)

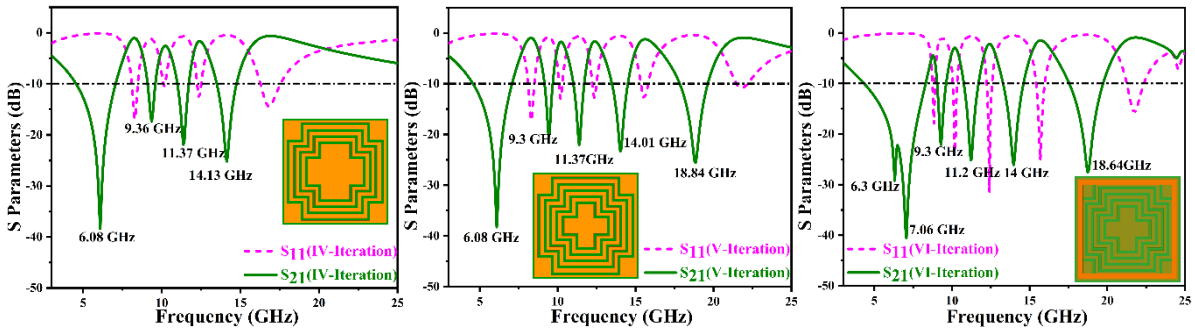

(d) (e) (f)

Fig. 3. S-parameters of the iterations of the proposed structure (a) I, (b) II, (c) III, (d) IV, (e) V, and (f) VI

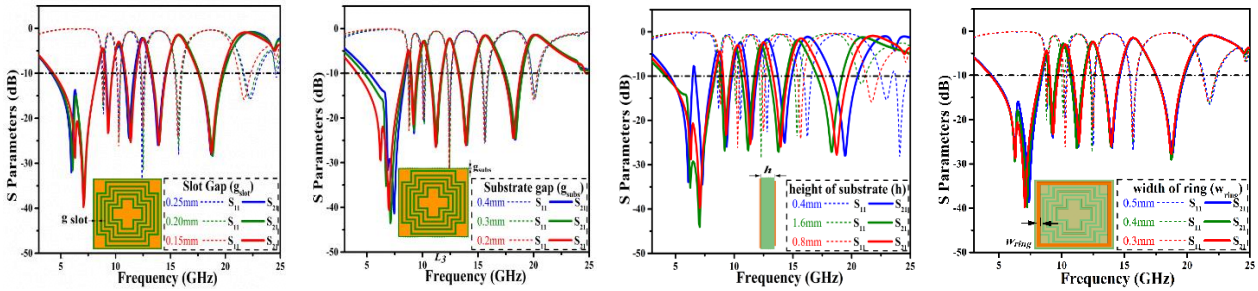

(a) (b) (c) (d)

Fig. 4. Frequency response varies with geometries (a) g_{slot} (b) g_{subs}, (c) height of substate (h), and (d) w_{ring}.

The upper conductive surface is only 6 mm × 6 mm, making the design that has been presented exceptionally space efficient. For this reason, the parametric research is restricted to only the optimal dimensions. So, to begin, the distance between the two slots (g_{slot}) was altered with a step size of 0.05 mm, ranging from 0.15 mm to 0.25 mm. Only the first band is affected when the spacing between slots is changed, and it demonstrates improved S_{21} performance at 0.15 mm; the other four bands are unaffected by the change. The relevant findings are shown in Figure 4(a).

As was discussed before, the frequency of the principal resonant mode is affected by the cross slot that is situated the farthest from the centre of the structure and has the largest perimeter. Therefore, changing the distance between the substrate and the higher conductive layer has only a significant impact on the first resonant band (g_{subs}). Figure 4(b) depicts the pertinent information.

The height of the substrate is yet another crucial component of the selective surface. Attenuation and bandwidth are both improved when the substrate thickness 'h' is set to 0.8 mm, as can be seen in Figure 4(c). Choosing a substrate thickness that is less than 0.8 mm not only restricts its use but also renders it unviable for space-constrained applications that are already on the market. One more parameter to take into consideration is the width of the square ring (w_{ring}), which is located in the lower conductive layer.

This should be set to 0.3 mm as the optimal value. Noticing that this ring is exactly the opposite of the first ring on the upper side, that is primarily responsible for the first band. Therefore, while narrowing the width of the ring, there was a discernible improvement in the S_{21} of the first band shown in Figure 4(d).

Each of the five concentric enclosed slots in the upper conductive layer of the proposed quintuple band FSS has a slot width of 0.22 mm, making up the total slot width of the upper conductive layer. The distance, marked by g_{slot}, that separates each of these slots has the same measurement as well, which is 0.15 mm. This distance is consistent across all of the slots. The unused area in the centre of the building resembles a four-legged loaded structure that has been optimized in terms of its dimensions. Whereas the lower conductive layer is made up of an optimized square ring that is positioned just beneath the first enclosed ring and has a width of w_{ring} equal to 0.3 mm. Additionally, the presence of this lower conductive ring contributes to the fact that the selectivity in the pass band range is increased.

Table 1: Iterations

No. of Iterations	Frequency Bands (GHz)	Resonant Frequencies (GHz)	Percentage Bandwidth (%)
I	4.70 - 7.14	6.31	41.2
II	4.48-7.00, 9.13-9.70	6.02, 9.41	44, 6.2
III	4.50-7.03, 9.0-9.62, 10.95-11.82	6.02, 9.36, 11.37	44, 6.6, 7.6

IV	4.55-7.06, 9.0-9.6, 10.99-11.72, 13.50-14.76	6.08, 9.36, 11.37, 14.13	43.2, 6.4, 6.5, 9
V	4.56-7.07, 9.0-9.68, 10.99-11.70, 13.40-14.60, 17.83-19.63	6.08, 9.3, 11.37, 14.01, 18.84	43.2, 7.3, 6.2, 8.5, 9.6
VI (Final)	4.34-8.30, 9.0-9.7, 10.76-11.80, 13.29-14.80, 17.55-19.73	6.3 & 7.06, 9.30, 11.20, 14.0, 18.64	62.6, 7.5, 9.2, 11, 11.69

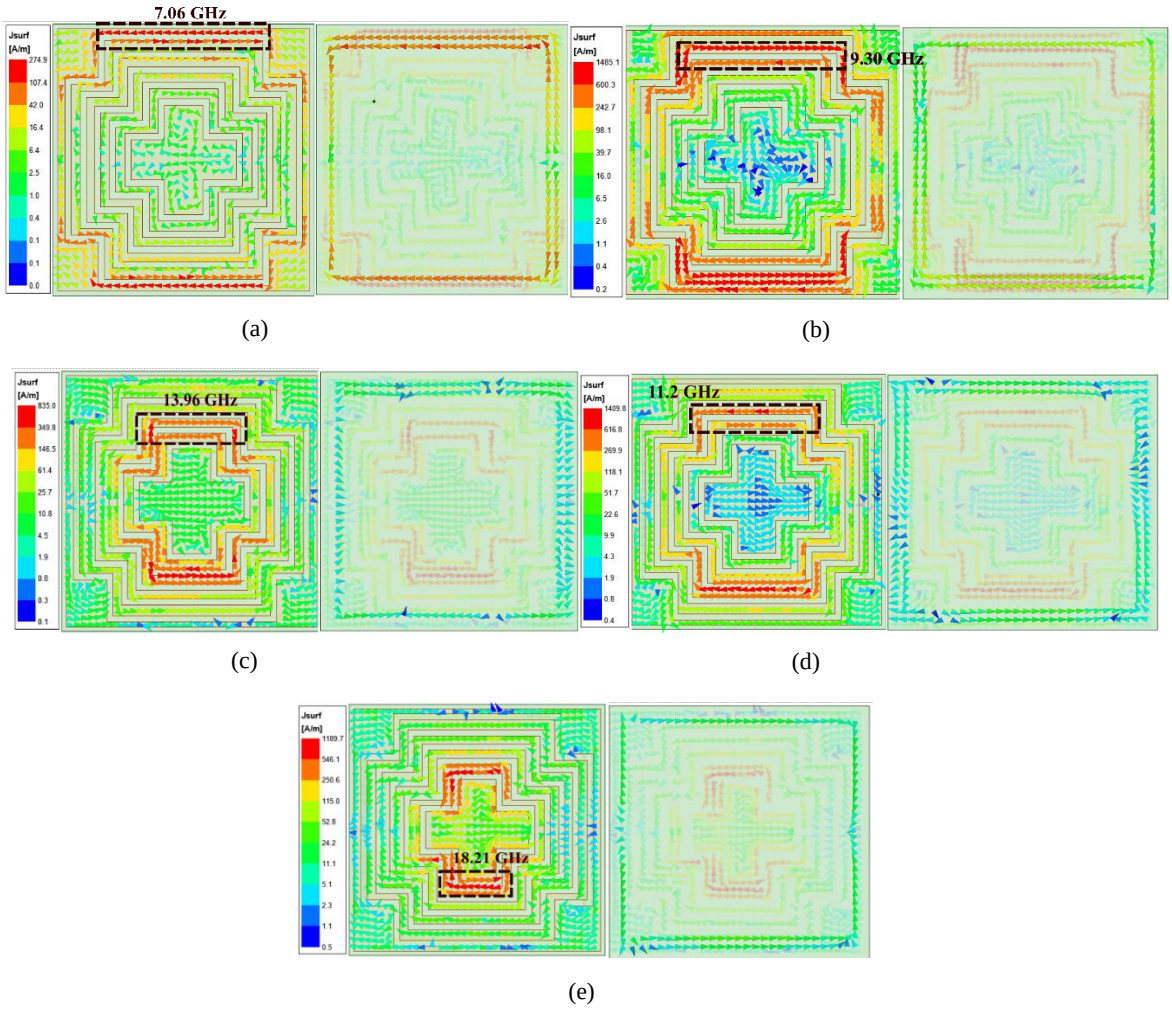

(a) (b)

(c) (d)

(e)

Fig. 5. Surface currents of the pentaband FSS (a) at the first resonance (7.06), (b) at the second resonance (9.30 GHz), (c) at the third resonance (11.20 GHz), (d) at the fourth resonance (14.20 GHz), and (e) at the fifth resonance (18.6 GHz)

Figure 5 illustrates that there is a substantial amount of surface current that flows in the opposite direction on the border of the slots. As a direct consequence of this, their individual stop bands are produced. In general, it is possible to draw the conclusion that each and every slot presents its stopband. Nevertheless, when creating periodic surfaces with many unit elements, it is necessary to take into account the mutual couplings that exist between the elements.

Now, the equivalent circuit is shown in Figure 6(a), considering a single ring, it can be broken down as follows. In the outermost ring, the two arms parallel to the E-fields will present a capacitance given by C_1. This is due to the capacitance between the metallic arms of the adjacent unit cells. In the same ring the other two arms will have an inductance given by L_1. The inductance L_1 in series with capacitance C_1 will provide a band-stop response. There will also be a small resistance offered by the arms (R_1). This completes the circuit on a single ring. Next, there will be a subsequent capacitance between two adjacent rings given by C_{c1}. This series can be repeated to obtain the final equivalent circuit model. There is a single ring on the bottom side of the substrate providing a band stop response. This has been modelled in series with the substrate (modelled as transmission line of length h). The structure is repeated for each ring taking into account the respective capacitances and inductances to generate the correct waveform of the full wave simulation shown in Figure 6(b). The circuit parameters are shown in Table 2.

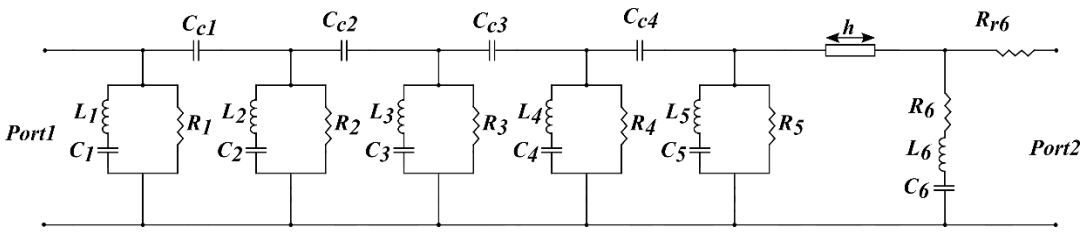

(a)

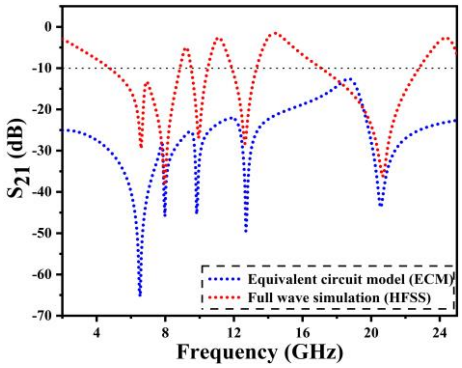

(b)

Fig. 6. (a) Equivalent circuit model and (b) comparison of S-parameters.

Table 2: Circuit parameters

	nH		pF		pF		ohm
L_1	1.43	C_1	0.39	C_{c1}	50	R_1	464
L_2	0.985	C_2	0.285	C_{c2}	50	R_2	129
L_3	0.975	C_3	0.21	C_{c3}	50	R_3	500
L_4	1.325	C_4	0.099	C_{c4}	50	R_4	500
L_5	0.43	C_5	0.18			R_5	500
L_6	0.001	C_6	0.115			R_6	20
						R_{r6}	0.001

4. Experimental verification

A finite prototype (Figure 7(a), 7(b)) consisting of 15 × 15 unit cells and having overall dimensions of 93 mm×93 mm is developed and tested in order to validate the findings that were reported in the preceding section. This technique requires appropriate horn antennas that are 145 cm (far field) away from the constructed pentaband structure that is mounted on a turn table for measurement under oblique incidence, and the structure is pivoted while the measurement is being carried out (Figure 7(c)).

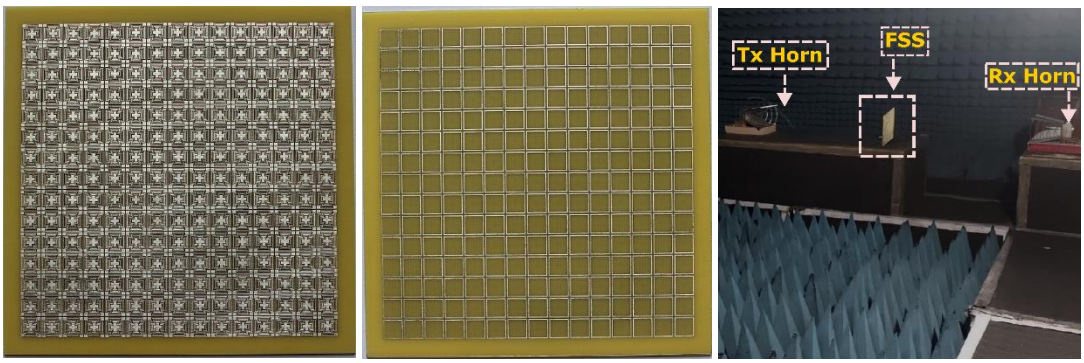

(a) (b) (c)

Fig. 7. Fabricated sample (a) front view, (b) rear view, and (c) measurement setup

The measurement is divided into two parts for convenience. First, the measurement of S_{21} is carried out between the two horn antennas without using the FSS. Second, the FSS prototype is utilized to determine the transmission coefficient that exists between the two horns. After then, the FSS-measured transmission is normalized based on how it compares to the data that was collected without it. The value of S_{21} is determined by measuring it at a number of different incidence angles for both TE and TM polarizations. Figure 8 presents the findings with respect to the standard error for (oblique) incident angles ranging from 0^0 to 75^0.

The structure exhibits a quintuple-band stop response, as shown in Figure 8, with resonance frequencies of 6.3 and 7.06, 9.30 and 11.2, 14.0 and 18.64 GHz. The fractional bandwidth is calculated as follows: 62.6, 7.5, 9.2, 11, and 11.69%.

The frequency response of the proposed FSS is unaffected by the wave's incident angle at any point in time. The FSS has been evaluated using a variety of polarization angles throughout the testing process. Because of its fourfold symmetry, the performance of the proposed element is nearly unaffected by the angles at which wave polarization occurs. Table 3 presents a comparison of the recently published works on pentaband FSS with the work that we intend to propose.

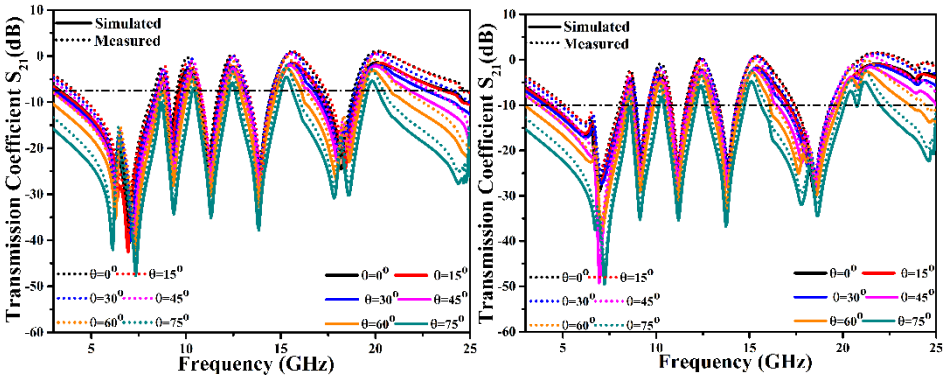

Fig. 8. Measured and simulated plot (a) TE polarization and (B) TM polarization.

Table 3: Comparison

Ref.	Cell dimensions (mm)	ϵ_r	Resonant frequency (GHz)	No. of layers	Angular stability	Minimum band ratio	Ratio of f_h/f_l	Symmetry
[20]	8.46 x 8.46 x 0.2	–	2.4, 3.38, 4.82, 6.32, 7.75	1	30	1.22	3.22	No
[21]	27 x 27 x 1.6	4.4	1.5, 1.8, 2.5, 3.5, 5.5	1	45	1.2	3.66	Yes
[22]	16 x 16 x 1.6	4.4	1.9, 2.46, 3.62, 5.42, 7.54	2	54	1.29	3.96	Yes
[23]	38 x 38 x 1.6	4.4	0.9, 1.5, 1.8, 3.5, 5.7	1	45	1.2	6.33	Yes
[24]	3.5 x 3.5 x 0.127	2.2	26.7, 29.8, 33.6, 38.1, 44.2	1	45	1.12	1.66	Yes
This work	**6.2 x 6.2 x 0.8**	**4.4**	**6.3 & 7.06, 9.30, 11.20, 14.0, 18.64**	**1**	**75**	**1.2**	**2.64**	**Yes**

The proposed FSS is characterized by the following salient characteristics:

- The proposed quintuple-band FSS for shielding applications is relatively compact ($0.08\lambda_0 \times 0.08\lambda_0 \times 0.012\lambda_0$), and can be used as a reflector or a shield in a number of different bands, including C, X, Ku, and K for specific applications.
- The presented selective layer, with its fourfold symmetry, exhibits an excellent polarization-insensitive response and high angular stability for both TE and TM modes up to 75^0. This is possible due to the layer's capacity to maintain a high degree of angular consistency. Additionally, the lowest frequency to highest frequency ratio is 2.64, and the lowest frequency to highest frequency ratio is 1.2.
- In the proposed design, we validated that the response of the equivalent circuit model was the same as the response of the full-wave simulation for the complete quintuple response. In comparison to the existing literature, the proposed design for the unit cell has a five-band response; yet, the ranges of these bands are relatively broad. Additionally, the size is quite diminutive.

5. Conclusion

A new low-profile single-layer FSS with a quintuple-band response structure has been introduced. In the suggested fourfold structural architecture, the upper conductive layer consists of five concentric cross slots, while the lower conductive layer is an optimized square ring. The stop bands' resonance frequencies are between 6.3 and 7.06, 9.30 and 11.2, and 14.0 and 18.64 GHz over the five bands. These frequencies have FBWs of 62.6%, 7.5%, 9.2%, 11%, and 11.6%. In addition, the structure's fourfold symmetry allows for a polarization insensitive response in both the TE and TM modes. This FSS can be utilized as a sub reflector for applications such as satellite systems (C band), EPR (electron paramagnetic resonance) spectrometers, motion and traffic light crossing detectors (X band), Direct Broadcast Satellite and broadcasting satellite service (Ku band), and short-range applications (K band).

References

[1] B. A. Munk, Frequency Selective Surfaces. New York: John Wiley & Sons, Ltd, 2000.
[2] P. Prasad, S. N. Singh, and A. Kumar, "Lightweight ultra-wideband antenna array equipped with thin frequency selective surface for high gain applications," Journal of Electrical Engineering, vol. 73, no. 6, pp. 396–404, 2022.
[3] S. Monni, A. Neto, G. Gerini, F. Nennie, and A. Tijhuis, "Frequency selective surface to prevent interference between radar and satcom antennas," IEEE Antennas and Wireless Propagation Letters, vol. 8, pp. 220–223, 2009.
[4] P. Taylor, A. Austin, E. Parker, M. Neve, J. Batchelor, J.-P. Yiin, M. Leung, G. Rowe, A. Williamson, and K. Sowerby, "Angular independent frequency selective surfaces for interference control in indoor wireless environments," Electronics Letters, vol. 48, no. 2, pp. 61–62, 2012.
[5] B. Sanz-Izquierdo, J.-B. Robertson, E. A. Parker, and J. C. Batchelor, "Wideband FSS for electromagnetic architecture in buildings," Applied Physics A, vol. 103, no. 3, pp. 771–774, 2011.
[6] G. H.-h. Sung, K. W. Sowerby, M. J. Neve, and A. G. Williamson, "A frequency-selective wall for interference reduction in wireless indoor environments," IEEE Antennas and Propagation Magazine, vol. 48, no. 5, pp. 29–37, 2006.
[7] C.-N. Chiu and W.-Y. Wang, "A dual-frequency miniaturized-element FSS with closely located resonances," IEEE Antennas and Wireless Propagation Letters, vol. 12, pp. 163–165, 2013.
[8] S. Çimen, "Novel closely spaced planar dual-band frequency-selective surface," IET Microwaves, Antennas & Propagation, vol. 7, no. 11, pp. 894–899, 2013.
[9] H. Fabian-Gongora, A. E. Martynyuk, J. Rodriguez-Cuevas, and J. I. Martinez-Lopez, "Active dual-band frequency selective surfaces with close band spacing based on switchable ring slots," IEEE Microwave and Wireless Components Letters, vol. 25, no. 9, pp. 606–608, 2015.
[10] M. Yan, J. Wang, H. Ma, S. Qu, J. Zhang, C. Xu, L. Zheng, and A. Zhang, "A quad-band frequency selective surface with highly selective characteristics," IEEE Microwave and Wireless Components Letters, vol. 26, no. 8, pp. 562–564, 2016.
[11] S. Yadav, M. M. Sharma, and R. K. Singh, "A polarization insensitive tri-band bandpass frequency selective surface for Wi-MAX and WLAN applications". Progress In Electromagnetics Research Letters, 101, pp.127-136, 2021.
[12] N. Liu, X. Sheng, C. Zhang, J. Fan, and D. Guo, "A miniaturized triband frequency selective surface based on convoluted design," IEEE Antennas and Wireless Propagation Letters, vol. 16, pp. 2384–2387, 2017.
[13] B. Sanz-Izquierdo, E. A. Parker, and J. C. Batchelor, "Dual-band tunable screen using complementary split ring resonators," IEEE Transactions on Antennas and Propagation, vol. 58, no. 11, pp. 3761–3765, 2010.
[14] C. Mias and C. Tsakonas, "Waveguide demonstration of varactor-diode tunable band-pass frequency-selective surface," Microwave and Optical Technology Letters, vol. 45, no. 1, pp. 62–66, 2005.
[15] Y.-M. Yu, C.-N. Chiu, Y.-P. Chiou, and T.-L. Wu, "A novel 2.5-dimensional ultraminiaturized-element frequency selective surface," IEEE Transactions on Antennas and Propagation, vol. 62, no. 7, pp. 3657–3663, 2014.
[16] M. Kartal, J. J. Golezani, and B. Doken, "A triple band frequency selective surface design for GSM systems by utilizing a novel synthetic resonator," IEEE Transactions on Antennas and Propagation, vol. 65, no. 5, pp. 2724–2727, 2017.
[17] N. Choudhary, A. Sharma, and S. Yadav, "A novel band stop frequency selective surface for the security of quad band mobile applications," in 2017 IEEE Applied Electromagnetics Conference (AEMC), 2017, pp. 1–2.
[18] B. Rahmati and H. R. Hassani, "Multiband metallic frequency selective surface with wide range of band ratio," IEEE Transactions on Antennas and Propagation, vol. 63, no. 8, pp. 3747–3753, 2015.
[19] R. A. Mellita, S. S. Karthikeyan, P. Damodharan, and D. S. Chandu, "A miniaturized quad-band frequency selective surface for c-band applications," Journal of Electromagnetic Waves and Applications, vol. 35, no. 14, pp. 1882–1893, 2021.
[20] A. Dey and R. Sanyal, "Single layer miniaturized ultra-thin FSS with five closely spaced bands," International Journal of Microwave and Wireless Technologies, vol. 11, no. 8, p. 797–805, 2019.
[21] S. Yadav, C. P. Jain, and M. M. Sharma, "Smartphone frequency shielding with penta-bandstop FSS for security and electromagnetic health applications," IEEE Transactions on Electromagnetic Compatibility, vol. 61, no. 3, pp. 887–892, 2019.

[22] A. Ghosh, M. Kumar, S. N. Islam, and S. Das, "Design and analysis of a compact penta-band polarization-insensitive bandstop frequency selective surface," IEEE Antennas and Wireless Propagation Letters, vol. 19, no. 1, pp. 59–63, 2020.
[23] U. Farooq, A. Iftikhar, M. F. Shafique, M. J. Mughal, A. Fida, and S. Khalid, "Polarization insensitive penta-bandstop frequency selective surface for closely placed bands," Microwave and Optical Technology Letters, vol. 63, no. 1, pp. 271–278, 2021.
[24] L. Martinez-Lopez, R. Martinez-Lopez, A. E. Martynyuk, J. Rodriguez- Cuevas, H. Fabian-Gongora, and J. I. Martinez-Lopez, "Close band spacing pentaband frequency selective surfaces based on concentric ring slots," IEEE Access, vol. 9, pp. 57 886–57 896, 2021.

Received 7 May 2023